J Mater Sci (2011) 46:136–144
DOI 10.1007/s10853-010-4873-x

Processing of chemical solution-deposited $BaTiO_3$-based thin films on Ni foils

Tanawadee Dechakupt · Song Won Ko · Sheng-Guo Lu · Clive A. Randall · Susan Trolier-McKinstry

Received: 12 July 2010 / Accepted: 25 August 2010 / Published online: 14 September 2010

Abstract $BaTiO_3$ films on base metal foils are of interest for capacitor applications, but the processing requires reducing atmospheres that influence the film defect chemistry and density. In this study, powders dried from barium titanate solutions and barium titanate films were studied by X-ray diffraction, differential scanning calorimetry, thermal gravimetric analysis, infrared spectroscopy, and spectroscopic ellipsometry at various points in the processing. It was found that atmospheres designed to minimize Ni oxidation delay decomposition of organics, leading to retained carbonate phases. Thus, crystallization of the barium titanate occurs via decomposition of a barium carbonate phase. Retained organics that are present during high temperature processing can cause porosity in the films. On annealing at 1000 °C, there is slightly increase in the refractive index of the film due to further crystallization and densification. The final refractive index is comparable to that of 95% dense barium titanate ceramics. Re-oxidation did not change the refractive index of the film over the wavelength range from 350 to 650 nm.

Introduction

Approximately 10^{12} multilayer ceramic capacitors (MLCCs) are made annually [1] using tape casting for the barium titanate and screen printing of the Ni electrodes. Over the last several decades, there have been major advances in optimization of the tape cast slurries and processes to obtain thinner green sheets [2–4]. At present, it is not clear what the ultimate lower bound of tape casting is; thus, investigation of thin film dielectrics prepared by alternative approaches becomes interesting.

High temperature-stable permittivities have been reported for chemical solution-deposited $BaTiO_3$-based thin films on metal foils [1, 5–7]. Recently, Aygun et al. [8] investigated the relationship between organic extraction and property development in chemical solution-deposited $BaTiO_3$ films on copper foils. They found that crystallization was retarded in reducing ambients when compared to higher P_{O_2} atmospheres. This was associated with the retention of organic residues. Improved microstructure and properties were obtained by tailoring the ramp rate on heating. Aside from that work, there is little information available on the evolution of the $BaTiO_3$ crystalline phase and organic removal at the low oxygen partial pressure conditions utilized in processing films on base metal foils. It should be noted that each metal foil requires different oxygen partial pressures to prevent metal oxidation per the Ellingham diagram, and so to obtain the best properties. Therefore, $BaTiO_3$ films on Ni foils, which are one of the primary material systems in commercial multilayer ceramic capacitors, were investigated in this study. Of particular concern is the fact that many of these films have not been formulated to optimize the blocking characteristics of the grain boundaries toward oxygen transport, as is typically done in multilayer ceramic capacitors [9]. Moreover, it is known that residual carbon can introduce very low local oxygen pressures [10–13], which in turn change the barrier at the film–electrode interfaces, and so may decrease the reliability. Thus, this study reports on the effect of the low temperature processing steps and organic

T. Dechakupt · C. A. Randall · S. Trolier-McKinstry
Materials Research Institute and Materials Science and Engineering Department, The Pennsylvania State University, University Park, PA 16802, USA

S. W. Ko (✉) · S.-G. Lu
Materials Research Institute, The Pennsylvania State University, University Park, PA 16802, USA
e-mail: swk10@psu.edu

removal on the evolution of the film depth profile, structural evolution, and crystallinity. Of particular interest was how the solvent system used for the film preparation, the initial pyrolysis conditions, and the crystallization steps affected the ultimate film quality. Transmission electron microscopy characterization of the film microstructure and interface quality is reported elsewhere [11].

Experimental procedure

In this study, $BaTiO_3$ thin films were prepared by chemical solution deposition, following procedures previously reported by Ihlefeld and Nagata [1, 6]. The precursors were batched in a glove box under an Ar atmosphere. First, barium acetate (99.999%, Sigma-Aldrich) was stirred in glacial acetic acid at 105 °C for 1 h, or until completely dissolved. In a separate flask, acetylacetone and titanium isopropoxide (99.99%, Sigma-Aldrich) were combined. Then, the dissolved Ba precursor was poured into the flask-containing Ti. The mixture of Ba and Ti precursors was allowed to react at 105 °C for 1 h. Two types of solution were then prepared. For one, methanol was added until a 0.1-M $BaTiO_3$ solution was obtained and then the solution was stirred at room temperature until homogenized. Alternatively, 0.2-M 2-methoxyethanol-based $BaTiO_3$ solution was prepared by distilling the reacted Ba and Ti mixture at 105 °C until the volume of the solution was approximately 10 mL, before re-diluting the solution to the desired molarity.

Before deposition, high purity Ni foil (25-μm thick, 99.99% Alfa Aesar) was pre-annealed at 900 °C in approximately 1×10^{-17} atm P_{O_2} to remove NiO and contamination. The $BaTiO_3$ solutions were spin-coated on the pre-annealed Ni foil at 3000 rpm for 30 s. Typically, after each deposition, the films were dried at 180 °C for 3 min and then 280 °C for 3 min on hotplates in air. In other cases, the drying temperature was varied. After every two spinning/drying steps, the films were heated to 350 °C for 1 min for further organic removal and then at 600–750 °C for 1 min under flowing N_2 gas (23 SLPM) in a rapid thermal annealer (RTA 600, Modular Process Technology Corp., San Jose, CA). Spinning, drying and RTA annealing were repeated until the desired number of layers was obtained. The films were then crystallized at 1000 °C for 1 h in 5×10^{-15} atm P_{O_2} in a reducing furnace and then re-oxidized at 600 °C for 30 min in 1×10^{-6} atm P_{O_2}. The heating rate of both steps in the reducing furnace was 5 °C/min. The P_{O_2} was controlled by a mixture of hydrogen, wet nitrogen (a gaseous mixture of nitrogen and water vapor) and dry nitrogen, and recorded monitored via an oxygen sensor in the tube furnace during heating and cooling.

Thermal gravimetric analysis (TGA) and differential scanning calorimetry (DSC) on the dried powders were carried out simultaneously on a TA Instruments SDT 2960 to examine the decomposition behavior of $BaTiO_3$ powders obtained from a solution. The $BaTiO_3$ solution was air-dried at 150 °C for 15 h. The powder was then heated to 900–1200 °C at a heating rate of 5 or 10 °C/min in either air or N_2 (flow rate set at 100 cc/min). To complement this study, dried $BaTiO_3$ powders were also calcined at different temperatures (500–900 °C) in air for 1 h and the phase content was identified by X-ray diffraction using a Scintag V X-ray diffractometer (Scintag Inc., Cupertino CA) with Cu Kα radiation. Data were collected from 20 to 60° 2θ with a step size of 0.02° and a 0.5 s acquisition time per step. A slow scan with a count time of 5 s per step was also used when a small amount of some phase, i.e., NiO, was expected. In order to investigate organic residue with processing conditions (pyrolysis temperature, pyrolysis duration, annealing atmospheres) in the films, Fourier transform infrared spectra were measured using a Nicolet NEXUS 670 FTIR spectrometer (Thermo Fisher Scientific Inc., Waltham, MA). Spectroscopic ellipsometry (SE) was used to determine the thickness, depth profile and optical constants of $BaTiO_3$ films on Ni foils, Si (Nova Electronic Materials), and sapphire (MTI Corporation) substrates. The instrument and the data modeling procedures are described elsewhere [14, 15]. The SE parameters, delta (Δ) and psi (Ψ), were collected at wavelengths from 250 to 750 nm with an increment of 5 nm at an incidence angle of 70°. Reference data were used for the optical properties where available. For unknown dielectric materials, a damped Sellmeier dispersion equation was used to describe the optical properties of the unknown phase [16, 17].

Results and discussion

Phase and microstructure development

Figure 1 showed X-ray diffraction patterns of a pre-annealed Ni foil and $BaTiO_3$ films RTA'd at different temperatures under flowing N_2. The film RTA'd at 600 °C shows an extremely low intensity of the $BaTiO_3$ 100 and 110 peaks, along with a trace amount of a second phase at a two-theta of 26.7°. The second phase peak corresponded to the highest peak of an oxycarbonate ($Ba_2Ti_2O_5CO_3$), which was reported to be an intermediate phase in the crystallization of perovskite $BaTiO_3$ [8, 18–21]. A recent article suggests that this intermediate phase may, in fact, contain very little Ti [22]. For the films RTA'd at 650–750 °C, the "oxycarbonate" phase disappears and slightly higher intensity $BaTiO_3$ peaks are shown. Since the electron diffraction pattern showed no sign of an amorphous phase

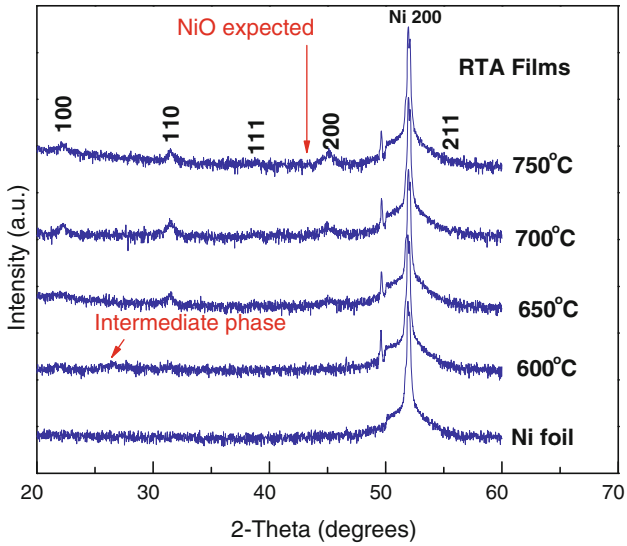

Fig. 1 XRD patterns of $BaTiO_3$ films on high-purity Ni foils RTA'd at different temperatures

(diffuse ring) [11], the low intensity of the RTA films is presumably due to the small crystallite size.

These same films were then annealed in a reducing atmosphere furnace at 1000 °C for 1 h. The XRD patterns after furnace annealing are shown in Fig. 2. The patterns for all films correspond to a well-crystallized polycrystalline pseudocubic perovskite phase with some degree of ⟨100⟩ orientation. The high intensity, narrow peaks for the furnace annealed films are a result of the larger grain size, compared to those of RTA'd films. The films heat-treated at 1000 °C possessed a dielectric constant of >1500 and dielectric loss of <0.03. These data were comparable to those described by Nagata [1].

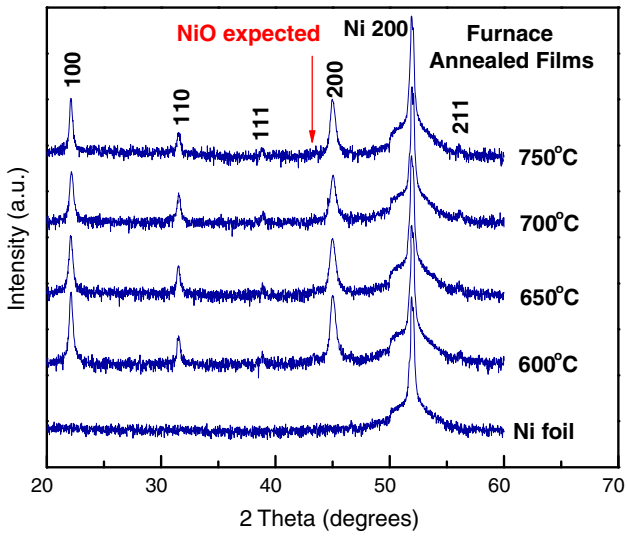

Fig. 2 XRD patterns of furnace annealed $BaTiO_3$ films that were RTA'd at different temperatures

There were no NiO peaks observed in the X-ray diffraction patterns of any of the RTA'd films. As described elsewhere [11], a NiO 200 peak was detected in slow scan X-ray diffraction of all furnace annealed and re-oxidized films. There is no significant trend in the amount of NiO for the furnace annealed films as a function of the RTA temperature.

Scanning electron microscopy was used to investigate the surface microstructure of furnace-annealed (1000 °C) $BaTiO_3$ films on Ni foils. The films are crack-free and consist of equiaxed grains with some porosity as shown Fig. 3. The porosity tends to decrease as the RTA temperature increases. It is believed that in an RTA step with flowing N_2, organic removal is incomplete (see below) and that porosity is developed when the film is subsequently furnace annealed. As has been described by Scherrer, in some solution-deposited films, if crystallization is initiated before densification is complete, the resulting films can incorporate porosity [23].

Organic decomposition

In order to improve the density of the films, a series of experiments was undertaken on the kinetics of organic removal. Figure 4 shows a comparison of the thermal analysis results in air and N_2 for powder-dried from a methanol-based $BaTiO_3$ solution. Clearly, the TGA curves measured in air and N_2 show complete decomposition at different temperatures (~750 °C for air flow and ~1000 °C for N_2 flow). The weight losses at 25–200 °C and 200–400 °C are due to evaporation of the solvent and absorbed moisture, and pyrolysis of organics, respectively. The major delay in the rate and amount of weight loss due to further organic removal for N_2 when compared to air is significant at temperatures of 400–600 °C. Figure 5 shows that powder calcined at 500 °C for 1 h in air consists of amorphous material along with $BaCO_3$ and either $Ba_2Ti_2O_5CO_3$ or the calcite-like $BaCO_3$. The formation of the intermediate phases reflected as a strong exothermic peak in the DSC curve (not shown here) in air, but as a small and broad peak in N_2. These phases have previously been reported as intermediate phases in $BaTiO_3$ crystallization [8, 18, 20, 21, 24–27]. Upon heating, crystallization continues (as witnessed by the higher intensity of the $BaTiO_3$ peaks) and the amount of the second phases gradually decreases. The oxycarbonate phase and $BaCO_3$ completely disappeared when the powder was calcined in air at 700 and 900 °C, respectively. It is believed that the last weight loss is due to decomposition of the carbonate phase. The DSC curve in N_2 shows extra peaks at 740 and 935 °C, compared to that in air. Thus, it is believed that the delay in weight loss is accompanied by slower carbonate decomposition and thus $BaTiO_3$ crystallization.

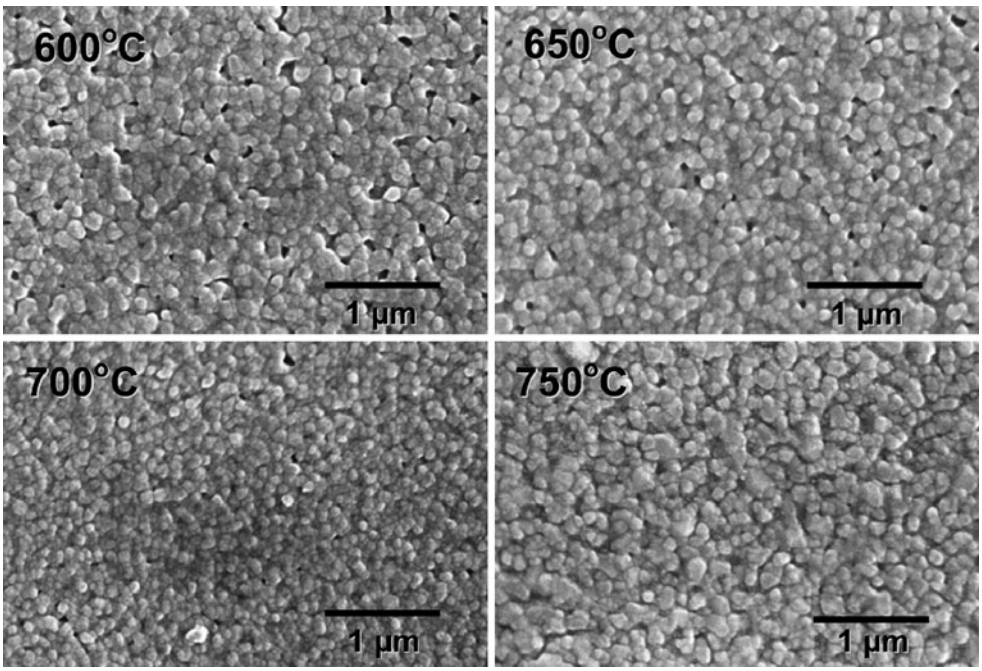

Fig. 3 Microstructure of furnace-annealed $BaTiO_3$ films that were RTA'd at different temperatures

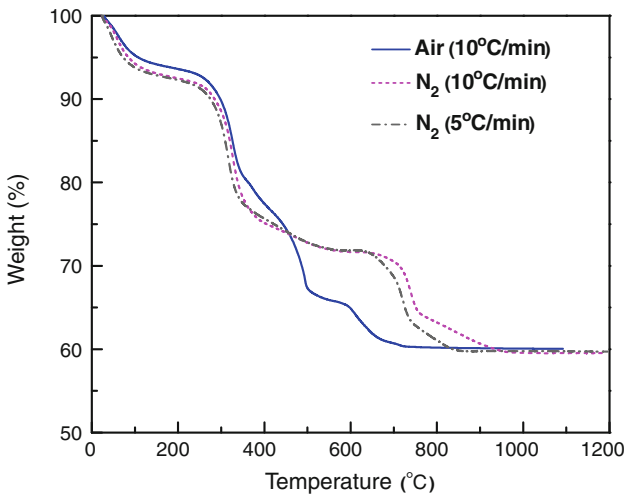

Fig. 4 TGA of dried powder from methanol-based $BaTiO_3$ solution

These results show that organic burn-out is delayed when there is insufficient oxygen available at elevated temperatures. Therefore, it is probable that $BaTiO_3$ films RTA'd at $\leq$750 °C in N_2 have residual organics that are ultimately the origin of the film porosity on subsequent furnace annealing at 1000 °C, especially as the heating rate in the RTA (60 °C/s) is much faster than that used in the thermal analysis experiment (5 or 10 °C/min). Although the slow heating rate used in the furnace annealing (5 °C/min) will assist organic removal, the low P_{O_2} might retard the process. The result is consistent with the observation of residual carbon in furnace-annealed $BaTiO_3$ films [11].

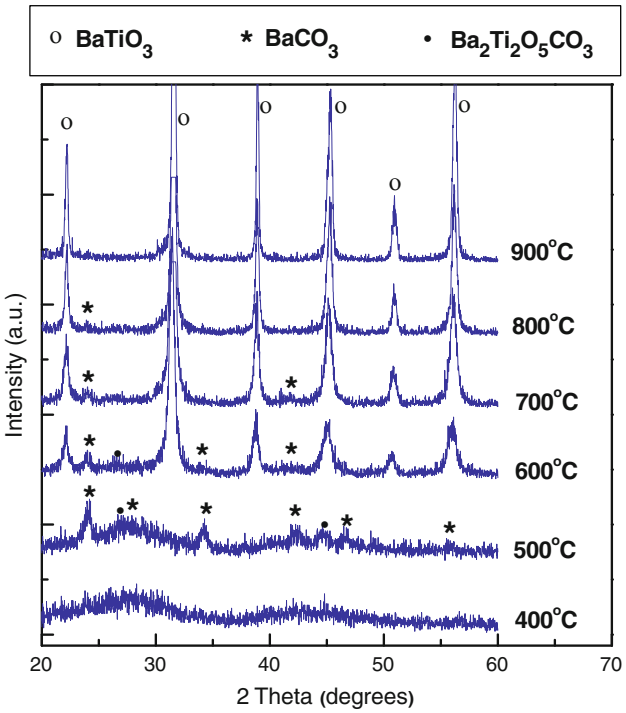

Fig. 5 XRD patterns of powders calcined in air at different temperatures

Thermal analysis and XRD patterns of the dried $BaTiO_3$ powder in air showed that the crystallization pathway from amorphous to perovskite $BaTiO_3$ occurred via a $BaCO_3$ or oxycarbonate ($Ba_2Ti_2O_5CO_3$) intermediate. In contrast,

$BaTiO_3$ thin films on Ni foil RTA'd at 600 °C show only a small amount oxycarbonate as an intermediate phase based on the XRD patterns shown in Fig. 1. This could be due to differences in surface area, heating rate, catalysis by the underlying Ni or substantial differences in the relative quantities of chemical precursor to furnace volume [8].

In air, the weight losses from powders prepared from methanol and 2-methoxyethanol solutions were completed at approximately the same temperature (700–750 °C for 2-methoxyethanol and 800 °C for methanol). In N_2, the completed decomposition of the 2-methoxyethanol-based powders is at 800 °C, which is much lower than that of the methanol-based powders. Therefore, 2-methoxyethanol-based solutions may be more suitable for processing in low P_{O_2} conditions.

In order to examine organic residues in films, $BaTiO_3$ films were prepared on Si substrates as function of pyrolysis temperature and time. Figure 6a shows FTIR spectra of $BaTiO_3$ films held at different temperatures for 5 min. For as-spin coated and 120 °C-treated $BaTiO_3$ films, peaks from the O–H bond (3300–3500 cm^{-1}), C–H bond (2880–3020 cm^{-1}), carboxylate (1560 cm^{-1}), carbonate (1420 cm^{-1}), Ti–O bond, and other organic molecular vibrations (498, 660, 793, 935, and 1034 cm^{-1}) are observed [28–30]. After pyrolysis in air at 390 °C, the peaks for the O–H and C–H bonds disappear and the intensity of the carboxylate peak decreases. Furthermore, the narrow and sharp carbonate peak at 1420 cm^{-1} changes to two broad peaks (1440 and 1390 cm^{-1}) with lower intensity. It is difficult to index the peaks because these absorption bands are broad, but the peaks could be attributed to the stretching vibrations of a carbonate complex [30, 31]. For films heated to 750 °C for 10 min in air, there is no carboxylate peak but carbonate peaks remain in Fig. 6b. The XRD pattern of a film annealed at 750 °C in N_2 atmosphere does not show $BaCO_3$ peaks, as shown in Fig. 1, but FTIR spectra of film annealed at 750 °C even in air indicate that the film contains $BaCO_3$. This is consistent with the XRD data of dried powders, e.g., the $BaCO_3$ peak was observed up to 800 °C.

Spectroscopic ellipsometry studies

Spectroscopic ellipsometry (SE) has previously been used to characterize the relative density, oxidation state and surface roughness of $BaTiO_3$ films and ceramics [32–38]. In this study, SE was used to track the evolution of $BaTiO_3$ films at different points during the processing. To avoid complications in data interpretation due to Ni surface roughness and Ni oxidation, Si and sapphire substrates were used for lower heat treatment temperatures. Finally, $BaTiO_3$ films on Ni foil were studied for higher temperature heat treatments.

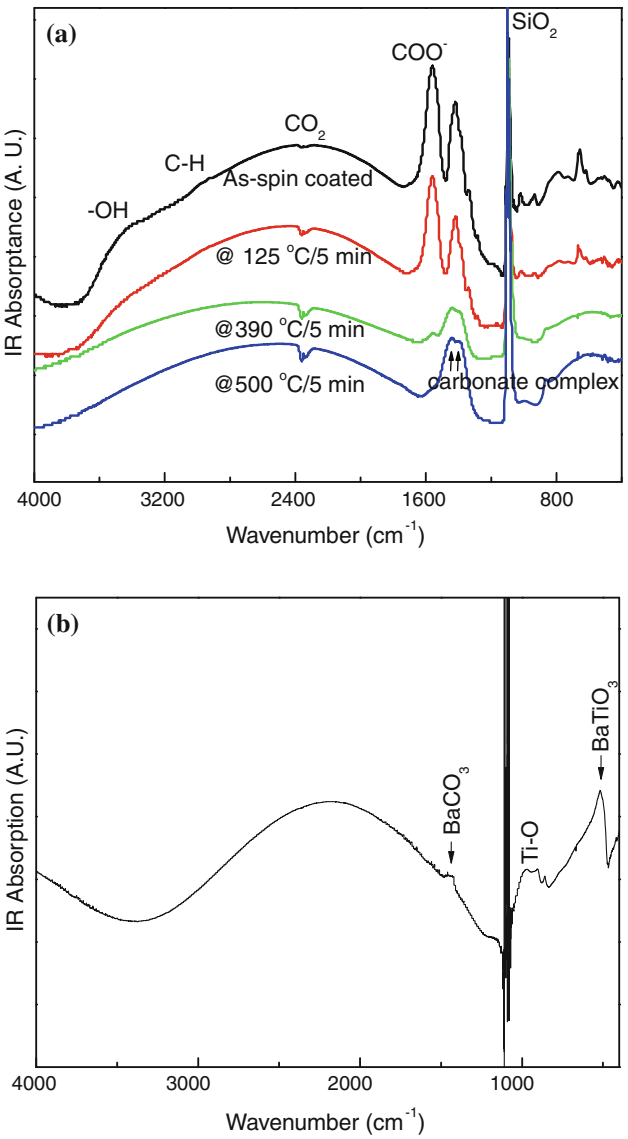

Fig. 6 FTIR spectra of **a** $BaTiO_3$ thin films as-spin coated, and pyrolyzed at 125, 390, and 500 °C for 5 min, and **b** FTIR spectra of $BaTiO_3$ thin film annealed at 750 °C for 10 min in air after pyrolysis

Amorphous-dried $BaTiO_3$ films

In this experiment, eight layers of 2-methoxyethanol-based $BaTiO_3$ solution (0.2 M) were deposited on a freshly etched Si wafer. Si was chosen for this study due to its excellent surface smoothness and its stability over this temperature range. After each layer deposition, the film was dried at different temperatures (200, 250, 300, 350 °C) for 5 min.

The best fit model for amorphous films on Si dried at different temperatures consisted of a bulk film with a thin layer of surface roughness. The sigma value describing the goodness of fit decreased from 0.089 to 0.038 with increasing drying temperature. Figure 7 shows the

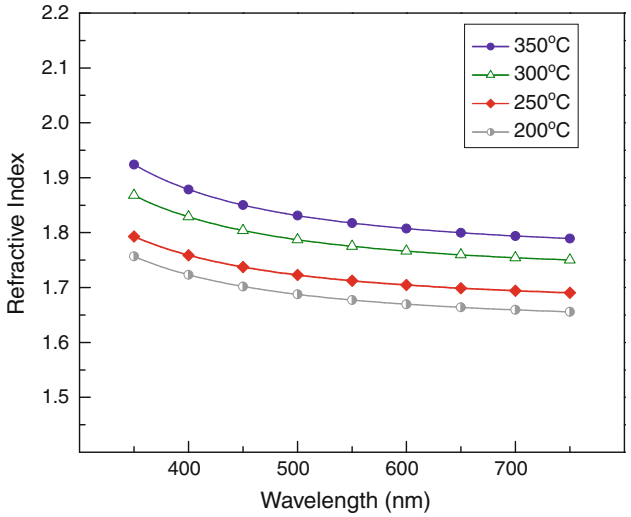

Fig. 7 Refractive index of dried amorphous $BaTiO_3$ films (prepared from a 0.2-M 2-methoxyethanol solution)

Table 1 Total thickness of amorphous $BaTiO_3$ films as a function of drying temperature (prepared from 0.2 M 2-methoxyethanol solutions)

Pyrolysis temperature (°C)	200	250	300	350
Total film thickness (Å)	5332 ± 64	4780 ± 89	4080 ± 26	3642 ± 8

measured refractive index of the densest region of each of the dried films. It can be seen that the refractive index increases as the films are densified at higher drying temperatures. Accordingly, Table 1 shows that the film thickness collapses from 5332 ± 64 to 3642 ± 8 Å after drying at 200 to 350 °C, respectively. The result is consistent with the TGA observation that a substantial fraction of the organics is lost in this temperature range.

$BaTiO_3$ films on sapphire substrates

2000-Å thick thin films were prepared and RTA'd at 750 °C in flowing N_2. A SE measurement was performed after the RTA annealing step (750 °C in N_2 flow). Then, SE data from the same film area were measured after the high temperature step (1000 °C, 10^{-15} atm P_{O_2}) and again after re-oxidation (600 °C, 10^{-6} atm P_{O_2}). An Al_2O_3 (0001) single crystal was used as the substrate because it provides a stable surface which will not complicate SE modeling. In addition, the Al_2O_3 single crystal substrate has a small thermal expansion mismatch with $BaTiO_3$ up to at least 1000 °C, giving crack-free films (7.5×10^{-6}/°C for Al_2O_3 and 9.8×10^{-6}/°C [39] for $BaTiO_3$). The data were collected using an achromatic compensator to minimize instrumental errors.

There are clear changes in the interference fringes of SE data after the 1000 °C step; however, no significant change was observed after re-oxidation. The SE data were modeled between 375 and 750 nm using Δ and Ψ, rather than tanΨ, cosΔ for σ. This typically enables better fitting of the depth profiles for all-transparent stacks, as discussed elsewhere [14].

Initially, modeling was performed with a two-layer structure consisting of a bulk film with some surface roughness. The two-layer model resulted in σ values that are unacceptably large (2.24°–3.44°). Much lower sigma (0.69°–0.81°) and improved fits were achieved when a low density layer was added at the film/substrate interface.

The optical properties at the three different stages in the processing are shown in Fig. 8. Obviously, the results after 1000 °C and after re-oxidation show comparable refractive indices and film depth profiles, suggesting that the re-oxidation step does not change the film substantially. The optical properties agree well with data for a ceramic sample with 95% density [40], meaning the film annealed at 1000 °C is fully crystallized and of reasonably high density. The RTA'd sample (750 °C) shows a lower refractive index. It can be seen that there may be some densification after the furnace annealing, although the change in thickness is within the 90% confidence limits

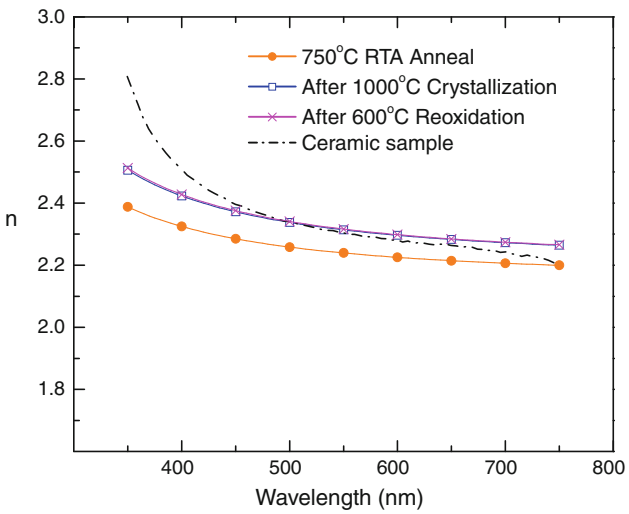

Fig. 8 Refractive index of RTA'd annealed, crystallized, and re-oxidized $BaTiO_3$ films

Table 2 Total thickness of $BaTiO_3$ films on (0001) Al_2O_3 after each annealing

Temperature (°C)	Total film thickness (Å)
750 (RTA)	2308 ± 43
1000 (crystallization)	2261 ± 91
600 (reoxidation)	2259 ± 94

(see Table 2). This suggests that the major increase in refractive index after furnace annealing may be due to further crystallization, rather than densification. The thickness of the surface roughness layer increases from 83.3 ± 1.8 Å (with fixed 50% air) for the RTA'd film to 206 ± 16 Å (with 32 ± 3% air) for the 1000 °C annealed film. The larger surface roughness of furnace annealed films is likely to be due to grain growth at high temperature. The result is consistent with the rough surface observed in the cross-sectional TEM sample [11].

$BaTiO_3$ films on Ni foil

In order to model the $BaTiO_3$/Ni interface, reference optical properties for the NiO were determined by spectroscopic ellipsometry from NiO obtained by heat-treating a high purity Ni foil at 600 °C in 10^{-6} atm P_{O_2} for 1 h. The resulting optical properties agree well with data for thermally oxidized NiO films from Lopez et al.'s work [41]. Figure 9 shows a comparison of the optical properties of the thermally grown NiO film on Ni foil from this experiment and a 95% dense $BaTiO_3$ ceramic. The primary difference between the two is in the imaginary part of the dielectric function.

The depth profiles and optical properties of $BaTiO_3$ films (on Ni foil) RTA'd at different temperatures (600–750 °C) were studied by spectroscopic ellipsometry (SE). Modeling of SE data was performed using reference data for Ni substrate and the thermally grown NiO. A Sellmeier oscillator was used to describe the optical properties of $BaTiO_3$ films. SE data were truncated to 350–650 nm to obtain reasonable models.

SE data of a $BaTiO_3$ film on Ni foil RTA'd at 750 °C was first modeled with various possible film structures, which at least consist of a bulk layer and surface roughness. It was found that an interface layer of either (oscillator + Ni) or pure NiO near the substrate results in good fits to the experimental data and similar sigma values were obtained (i.e., 0.081 for mix of oscillator and Ni and 0.078 for pure NiO). It is noted that the $BaTiO_3$ film refractive index extracted from both the models is the same and comparable to that of a $BaTiO_3$ ceramic sample. The large sigma is mainly due to error in the experimental data when delta is close to 0 and 180°. Fits of delta and psi for the two-model structures are shown in Fig. 10.

Although the model with a NiO interface shows a slightly better fit for this specific film, the resulting depth profile is not realistic. The thickness of the $BaTiO_3$ film is 1026.6 ± 65.3 Å, which is approximately half of the total

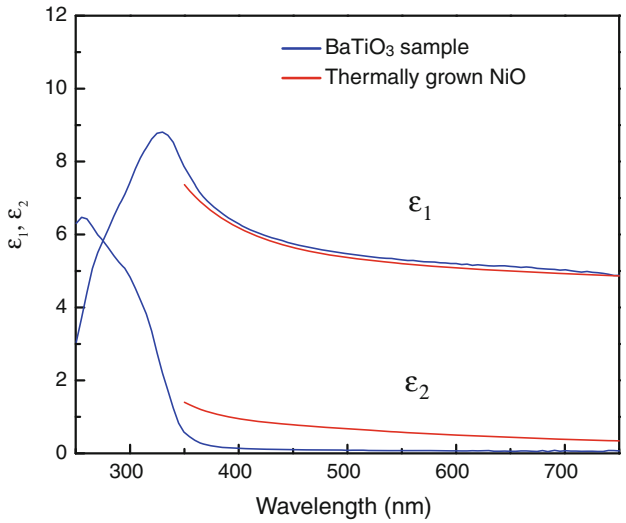

Fig. 9 Dielectric function of the thermally grown NiO and a $BaTiO_3$ ceramic sample

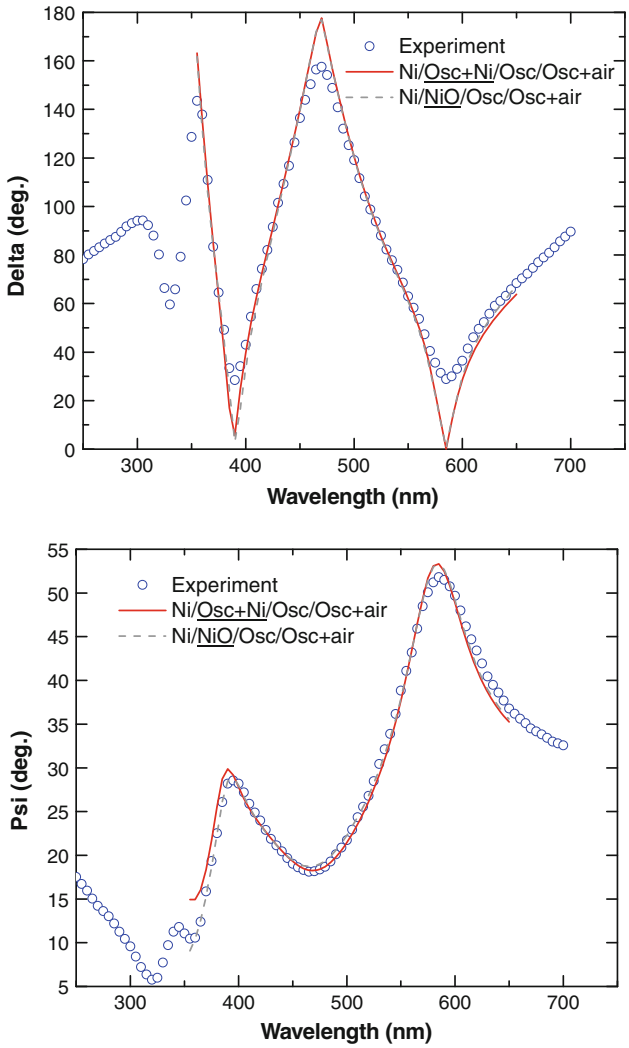

Fig. 10 Model fits of 750 °C RTA'd $BaTiO_3$ film on high-purity Ni foil

thickness of the film with the same number of spin-coated layers (8 layers) on (0001) Al_2O_3. In addition, the NiO layer is quite thick (902.9 ± 49 Å), which is in disagreement with the fact that XRD did not detect NiO peak on this same film. As was previously described, the refractive indices of $BaTiO_3$ and NiO are quite similar. Thus, it is believed that the "NiO" is simply an artifact created by the model's attempts to create a slightly more optically lossy $BaTiO_3$ film. A similar situation also occurred on modeling other RTA'd films. Thus, it is believed that the model without NiO at the interface is correct for all RTA'd films.

Depth profiles for the best fit models (without NiO) of $BaTiO_3$ films RTA'd at other temperatures modeled show a reasonable thickness of $BaTiO_3$ with a rough interface between the Ni and the $BaTiO_3$. For example, the total thickness of the 750 °C RTA'd $BaTiO_3$ is 1984 ± 242 Å and at the film substrate/interface film there is a 343 ± 106 Å thick layer with 9 ± 5 vol.% of Ni mixed in the $BaTiO_3$ film. The thickness of this layer agrees well with the rms roughness (37 nm) of the pre-annealed Ni foil, suggesting that this layer is due, at least in part, to the surface roughness of the Ni foil. It is noted that the 600 °C RTA'd film does not show surface roughness on the $BaTiO_3$, suggesting that the majority of the surface roughness develops at higher temperatures. In addition, the best fit without a NiO interface agrees well with the XRD results and cross-sectional TEM studies on RTA'd films, which showed no detectable NiO.

Figure 11 and Table 3 show the refractive index and total thickness, respectively, of $BaTiO_3$ films on Ni RTA'd at different temperatures. It can be seen that as the RTA temperature increases, further densification and film crystallization occur, resulting in a higher refractive index for the $BaTiO_3$ film. The film thickness decreases after annealing at 600 or 650 °C and becomes stable above 700 °C.

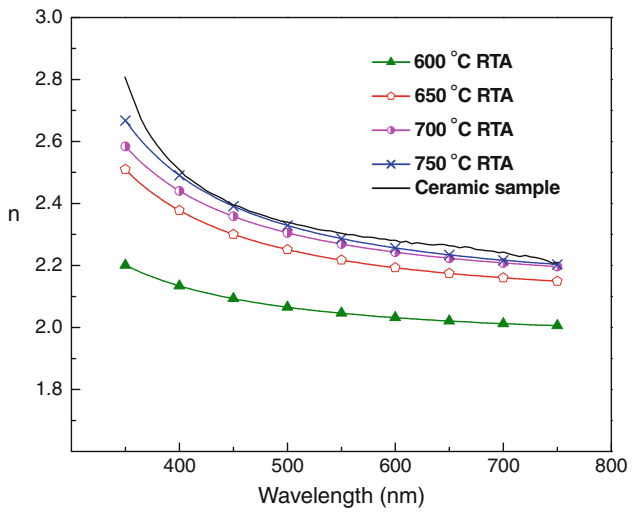

Fig. 11 Refractive index of RTA'd $BaTiO_3$ films on high-purity Ni foil

Table 3 Total thickness determined by SE for $BaTiO_3$ films on high purity Ni foil as a function of RTA temperature

RTA temperature (°C)	600	650	700	750
Total film thickness (Å)	2262 ± 268	2066 ± 215	1970 ± 296	1959 ± 230

Conclusions

Since high-temperature annealing of $BaTiO_3$ films on base metal foils is performed at low oxygen partial pressures, organic decomposition for powders dried from barium titanate solutions and barium titanate films was studied. It was shown that complete decomposition of organics in N_2 flow is extended to higher temperatures, compared to that in air. Thus, when fast heating rates are used, as in an RTA (60 °C/s), residual carbon is expected. The retained organics can cause porosity development during the high-temperature annealing. The presence of residual organics was confirmed in the cross-sectional TEM study [11].

Spectroscopic ellipsometry was used to track the evolution of film thickness, optical properties and film density as a function of the processing conditions. The decrease in thickness as a function of drying temperature is consistent with the weight loss observed in TGA results. The refractive index of the films increases as the RTA temperature increases, suggesting further crystallization of barium titanate and organic decomposition. The furnace-annealed (1000 °C) films show a refractive index comparable to that of a 95% dense ceramic.

Acknowledgements This study was financially supported by a Royal Thai government scholarship, Intel Corporation, and Kemet Electronics.

References

1. Nagata H, Ko SW, Hong E, Randall CA, Trolier-McKinstry S, Pinceloup P, Skamser D, Randall M, Tajuddin A (2006) J Am Ceram Soc 89(9):2816
2. Yosenick TJ, Miller DV, Kumar R, Nelson JA, Randall CA, Adair JH (2005) J Mater Res 20(4):837
3. Pithan C, Hennings D, Waser R (2005) Int J Appl Ceram Technol 2(1):1
4. Song YL, Liu XL, Zhang JQ, Zou XY, Chen JF (2005) Powder Technol 155(1):26
5. Dawley JT, Clem PG (2002) Appl Phys Lett 81(16):3028
6. Ihlefeld J, Laughlin B, Hunt-Lowery A, Borland W, Kingon A, Maria J-P (2005) J Electroceram 14(2):95

7. US Patent (2006) 7,029,971
8. Aygun SM, Daniels P, Borland WJ, Maria J-P (2010) J Mater Res 25(3):427
9. Tsur Y, Dunbar TD, Randall CA (2001) J Electroceram 7:25
10. Nishida K, Kishi H, Funakubo H, Takeuchi H, Katoda T, Yomamoto T (2007) Jpn J Appl Phys 46:7005
11. Dechakupt T, Yang G, Randall CA, Trolier-McKinstry S, Reaney IM (2008) J Am Ceram Soc 91(6):1845
12. Yang GY, Dickey EC, Randall CA, Barber DE, Pinceloup P, Henderson MA, Hill RA, Beeson JJ, Skamser DJ (2004) J Appl Phys 96(12):7492
13. Yang GY, Lee SI, Liu ZJ, Anthony CJ, Dickey EC, Liu ZK, Randall CA (2006) Acta Mater 54:3513
14. Gibbons BJ, Trolier-McKinstry S (1997) IEEE Trans Appl Supercond 7(2):2177
15. Trolier-McKinstry S, Hu H, Krupanidhi S, Chindaudom P, Vedam K, Newnham RE (1993) Thin Solid Films 230:15
16. McKinstry S (1992) Characterization of ferroelectric surfaces and thin films by spectroscopic ellipsometry, Ph.D. Thesis, The Pennsylvania State University, University Park
17. Tompkins HG, McGahan WA (1999) Spectroscopic ellipsometry and reflectometry: a user's guide. Wiley, New York
18. Frey MH, Payne DA (1995) Chem Mater 7(1):123
19. Duran P, Gutierrez D, Tartaj J, Banares MA, Moure C (2002) J Eur Ceram Soc 22(6):797
20. Kumar S, Messing GL, White WB (1993) J Am Ceram Soc 76(3):617
21. Hoffmann S, Waser R (1999) J Eur Ceram Soc 19(6–7):1339
22. Ischenko V, Pippel E, Koferstein R, Abicht HP, Woltersdorf J (2007) Solid State Sci 9(1):21
23. Scherer GW (1997) J Sol-Gel Sci Technol 8(1-3):353
24. Lee B, Zhang JP (2001) Thin Solid Films 388(1–2):107
25. Mao CL, Dong XF, Zeng T (2007) Mater Lett 61(8-9):1633
26. Veith M, Mathur S, Lecerf N, Huch V, Decker T, Beck HP, Eiser W, Haberkorn R (2000) J Sol-Gel Sci Technol 17(2):145
27. McCauley DE, Chu MSH, Megherhi MH (2006) J Am Ceram Soc 89(1):193
28. Frey MH, Payne DA (1995) Chem Mater 7:123
29. Kamalasanan MN, Kumar ND, Chandra S (1994) J Appl Phys 76(8):4603
30. Stockenhuber M, Mayer H, Lercher JA (1993) J Am Ceram Soc 76(5):1185
31. Little H (1966) Infrared spectra of adsorbed species. Academic Press, London, New York, p 77
32. Jellison GE, Boatner LA, Lowndes DH, McKee RA, Godbole M (1994) Appl Opt 33(25):6053
33. Ianculescu A, Gartner M, Despax B, Bley V, Lebey T, Gavrila R, Modreanu M (2006) Appl Surf Sci 253(1):344
34. Huang ZM, Xue JQ, Ge YJ, Qin JH, Hou Y, Chu JH, Zhang DH (2006) Appl Phys Lett 88(21):212902
35. Tsurumi T, Harigai T, Tanaka D, Kakemoto H, Wada S (2004) Sci Technol Adv Mater 5(4):425
36. Hu ZG, Wang GS, Huang ZM, Chu JH (2003) J Phys Chem Solids 64(12):2445
37. Pita K, Cheng SD, Kam CH, Zhou Y, Lam YL, Chan YC (1999) Ferroelectrics 231(1–4):655
38. Nenkov M, Pencheva T (1988) Thin Solid Films 324(1–2):305
39. Jaffe B, Cook W R Jr, Jaffe H (1971) Piezoelectric ceramics. Academic Press, London, New York
40. Biegalski M, Trolier-McKinstry S (2005) J Am Ceram Soc 88(1):71
41. Lopez-Beltran AM, Mendoza-Galvan A (2006) Thin Solid Films 503(1-2):40